Scanning Confocal Optical Microscopy and Magnetic Resonance on Single Defect Centers

A. Gruber, A. Dräbenstedt, C. Tietz, L. Fleury, J. Wrachtrup,* C. von Borczyskowski

The fluorescence of individual nitrogen-vacancy defect centers in diamond was observed with room-temperature scanning confocal optical microscopy. The centers were photostable, showing no detectable change in their fluorescence emission spectrum as a function of time. Magnetic resonance on single centers at room temperature was shown to be feasible. The magnetic resonance spectra revealed marked changes in zero-field splitting parameters among different centers. These changes were attributed to strain-induced differences in the symmetry of the centers.

Spectroscopy on single quantum systems promises to become a powerful method for the investigation of impurities in the condensed phase. The development of high-resolution optical microscopy has fostered considerable progress in this field. Most prominent studies use near-field (*1–4*) and confocal fluorescence microscopy (*5*) on single dye molecules. Individual mesoscopic systems such as quantum dots have been investigated in a similar way (*6*, *7*). There is a continuous demand to extend the class of systems that can be investigated with these techniques, especially to technologically relevant materials. Here we report the observation of defect or color centers on an individual basis. The centers detected were nitrogen vacancy (N-V) defects in diamond. Diamond has been subject to extensive optical investigations, and over 100 luminescent defects have been reported to exist (*8*, *9*). The N-V center is one of those studied in most detail (*10–12*). It consists of a substitutional nitrogen atom with an adjacent carbon vacancy (*13*) and has C_{3v} symmetry, with the symmetry axis oriented along the crystallographic [111] axis (*14*). The main photophysical parameters of the N-V center have been determined previously (*15*) and indicate the suitability of the system for single center detection; they are a large absorption cross section at the excitation wavelength, a short excited-state lifetime τ [for synthetic type 1b diamond τ = 11.6 ns (*16*)], and high quantum efficiency ($\phi \approx 1$) (*15*) for radiative relaxation. In addition, no efficient shelving in a metastable state has been reported for N-V centers at room temperature, although the high spectral hole-burning efficiency at low temperature indicates their existence (*12*). It is of considerable importance for the present study that the center is assumed to have a paramagnetic electron ground state (*11*), making it accessible to optically detected magnetic resonance (ODMR).

N-V centers are most efficiently created in type 1b synthetic diamond through electron irradiation (2 MeV) and subsequent annealing at 900°C in vacuum (*10*). Single diamond crystals of 100 μm thickness were used in our experiments. Electron (e) irradiation doses between 10^{12} e/cm^2 and 10^{15} e/cm^2 and annealing times around 1 hour yielded defect center concentrations of 0.2 to 200 centers per cubic micrometer, allowing us to resolve individual centers at the lowest radiation doses.

The sample fluorescence was excited and probed with a self-built confocal optical microscope operating at room temperature (*17*). Sets of lateral scans of dimensions 20 by 20 μm^2 were obtained for diamond samples irradiated with different electron doses, decreasing from 5×10^{14} e/cm^2 (Fig. 1A) to 1×10^{13} e/cm^2 (Fig. 1C). The axial position of the excitation focus was chosen to be 50 μm below the surface of the diamond. The fluorescence intensity decreases with decreasing radiation dose, thus diminishing the defect center density. In Fig. 1C, the concentration of luminescent centers is such that the average distance between them is larger than the diameter of our probe volume. A 5 by 5 μm^2 scan of the lower left corner of Fig. 1C (Fig. 1E) clearly demonstrates the resolution of individual luminescent spots. The full width at half maximum (FWHM) of the spots (see Fig. 1D) is 330 nm, which is close to the diffraction-limited spatial resolution of our confocal microscope. When the electron irradiation dose was further decreased, this spot size remained constant but the average distance between the spots increased. We conclude that we observed individual quantum constituents of the diamond lattice. Under similar electron irradiation and annealing conditions as those used in our experiment, other types of luminescent defect centers have been reported to exist in diamond (*15*). In order to identify the defect, we recorded the fluorescence spectra of individual luminescent centers found in our experiments (Fig. 2). The observed spectrum agrees well with recent low-tempera-

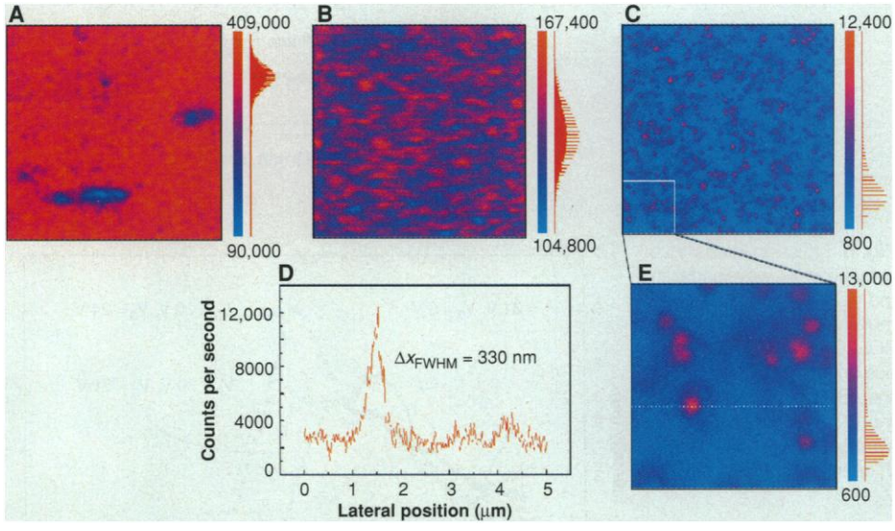

Fig. 1. Confocal microscopy raster scans (20 by 20 μm^2) of diamond samples irradiated with different electron doses. The bars on the right side of each figure define the colors in terms of counts per second. The numbers on the bottom and top of each bar give the minimum and maximum number of counts per second found in that scan. (**A**) Electron radiation dose 5×10^{14} e/cm^2, (**B**) dose 1×10^{14} e/cm^2, (**C**) dose 1×10^{13} e/cm^2. (**E**) Scan (5 by 5 μm^2) of the lower left corner of (C). (**D**) Line scan along the dotted line in (E). Δx_{FWHM} indicates the full width at half maximum of the fluorescence spots in (E). In all of the experiments, the laser intensity impinging on the sample was 9 μW, and the dwell time per pixel was 10 ms.

Institute of Physics, University of Technology Chemnitz, Reichenhainer Strasse 70, 09126 Chemnitz, Germany.

*To whom correspondence should be addressed. E-mail: wrachtru@physik.tu-chemnitz.de

ture bulk fluorescence spectra of the same system (*10*), proving that the observed fluorescence stems from a N-V defect center.

Even under the highest excitation intensities used (5 MW/cm^2) (*18*), none of the centers investigated so far showed any indication of photobleaching or any change in the fluorescence spectrum as a function of time. However, intensity fluctuations on a time scale around 10 μs have been observed with the intensity autocorrelation function (*19*). The correlation time depends on the excitation power. This is a further hint at the existence of a metastable state in the optical pumping cycle of the center (*20*).

Previous high-resolution optical (*11*, *12*) and electron paramagnetic resonance measurements (*20*) have revealed the spin triplet nature (total spin angular momentum $S = 1$) of the electronic ground state of the N-V center. The first excited triplet state (^{3}E) is believed to be populated through optical excitation from the ground state (^{3}A). On the basis of low-temperature optical investigations, it has been concluded that the optical pumping cycle of the N-V center, involving triplet-triplet absorption, internal conversion, and fluorescence relaxation, does not conserve spin angular momentum (*21*), leading to spin-selective population of the ground triplet substates of the excited defects. Thus, continuous optical excitation is believed to generate a non-Boltzmann steady-state spin alignment in the N-V center in the triplet ground state. The degeneracy of the spin sublevels of this triplet ground state is lifted because of the anisotropic dipolar interaction of the unpaired electron spins. Without applying an external magnetic field, the concomitant splitting is described by the two zero-field splitting parameters D and E (*22*). The parameter E can be interpreted as a measure of the axial symmetry of the center (*23*). Microwave radiation resonant with the triplet spin transitions in the ground state affects the steady-state population of the optically pumped ^{3}E-state of the N-V defect center. The ensuing change in fluorescence intensity is representative of the magnetic resonance in the triplet ground state. This ODMR signal has previously been observed at low temperature (*24*). The activation energy for spin lattice relaxation (time constant T_1 = 1.170 ms) has been determined to be 62.2 meV (*20*). If the optical pumping cycle is fast enough, one would thus expect to find spin alignment in the ground state and consequently an ODMR signal even at room temperature. The magnetic resonance signal of an ensemble of defect centers ($n \approx 10$) obtained under ambient conditions (Fig. 3A) was indeed found to appear as a 10% decrease of the fluorescence intensity of the centers. Two nearly degenerated lines were obtained, with a splitting between the maxima of the two components of $2E$ = 14 MHz and a width of ≈12 MHz for each line. On the basis of known zero-field splitting parameters of the N-V center (*24*) (Table 1), the two ODMR lines can be attributed to two of the three possible transitions in the ground triplet state. The observation of two ODMR lines in the ensemble spectra indicates that the local axial symmetry (C_{3v}) of most of the centers is broken in the ground state (*23*). In the ODMR spectrum of a single center (Fig. 3C), only a single line is observed. A best fit to the spectrum yields a Lorentzian curve (line width 5 MHz) at 2870 MHz. This is expected for a center with an E value close to or equal to zero, so that no splitting can be resolved in the ODMR spectrum. The center obviously has retained axial symmetry. In contrast, the ODMR spectrum of a different single center (Fig. 3B) shows two lines, each with a width of 5 MHz and a splitting of ≈4 MHz. Obviously, the axial symmetry of this center is broken. Only 15% of the centers observed showed a single ODMR line and thus had axial symmetry. Most of the centers had E values ranging from 2 to 9 MHz. This explains why the ODMR signal of symmetric centers is usually masked in bulk magnetic resonance studies, where we always found a two-line spectrum. Recent magnetic resonance experiments on the excited triplet state of single molecules (*25*–*27*) at low temperature showed ODMR lines that were inhomogeneously broadened. The Lorentzian line shape found in our experiments on single centers may be due to the fact that at room temperature, the shortening of the transversal spin relaxation time T_2 causes a homogeneous broadening larger than the hyperfine coupling, giving rise to an overall homogeneous ODMR line.

Because of its optical, mechanical, and electronic properties, diamond is a material of considerable interest for numerous industrial applications. Most of the diamond material used in industrial applications is grown by chemical vapor deposition, resulting in microcrystalline material (*8*). Confocal fluorescence microscopy (as demonstrated here) or near-field microscopy will provide new insight into the properties of such types of diamond. The present studies were carried out at room temperature, and the

Table 1. Comparison of the zero-field splitting parameters D and E between different centers at room temperature as well as with low-temperature (T = 1.5 K) bulk measurements.

Zero-field splitting parameters	D/MHz	E/MHz
Ensemble (T = 300 K)*	2870	7.0 ± 0.1
Ensemble (T = 1.5 K)†	2880	7.5
Center 1* (T = 300 K)	2870	0 ± 0.7
Center 2† (T = 300 K)	2870	2 ± 0.4

*This work. †Reference (*23*).

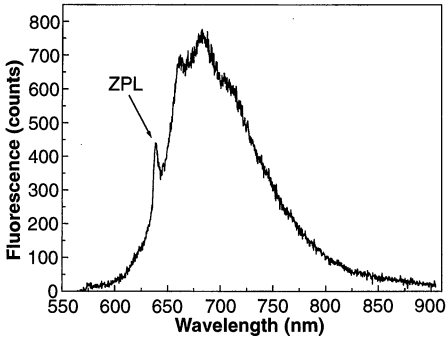

Fig. 2. Fluorescence spectrum of a single N-V defect center. The wavelength of the zero phonon line (ZPL) is 637 nm (1.945 eV). Excitation was at 514 nm. Accumulation time was 600 s. A holographic notch and red pass filter were used to suppress stray light.

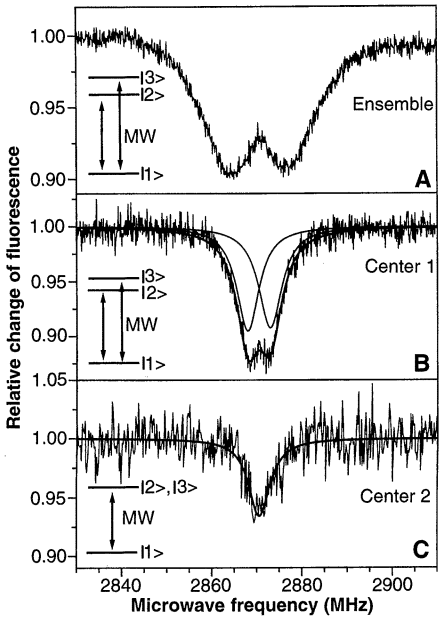

Fig. 3. Optically detected magnetic resonance spectrum of an ensemble of N-V centers (**A**) and two different single N-V centers (**B** and **C**) in zero external magnetic field. Accumulation times were 120 s for the ensemble spectrum, 600 s for center 1, and 800 s for center 2. For the ODMR experiment on center 2, the optical excitation intensity was four times greater than that used on center 1. The smooth curves superimposed on the data in (B) and (C) are fits with Lorentzian lines. The resulting zero-field splitting parameters are listed in Table 1. The insets show the spin sublevels in the ^{3}A ground state of the center, labeled |1>, |2>, and |3>. The arrows indicate the microwave (MW) irradiation.

key components of our microscope are standard items in commercial product lines. This will make the technique easily accessible to a large community of materials scientists. The limited optical spectral resolution resulting from the large room-temperature zero phonon linewidth (FWHM = 30 cm^{-1} at $T = 300$ K) can be partly overcome by magnetic resonance. Such ODMR spectra contain a great variety of structural information; for example, on the distribution of other impurities around the center (*24*) or the local strain in the diamond lattice, as demonstrated here. More sophisticated ODMR experiments, including the use of ultrahigh magnetic field gradients (*28*) and ground-state nuclear magnetic resonance experiments, can be envisaged. The combination of these techniques with optical microscopy allows detailed material characterization at a local level that is otherwise masked by ensemble averaging.

REFERENCES AND NOTES

1. E. Betzig and R. J. Chichester, *Science* **262**, 1422 (1993).
2. X. S. Xie and R. C. Dunn, *ibid.* **265**, 361 (1994).
3. W. P. Ambrose, P. M. Goodwin, J. C. Martin, R. A. Keller, *ibid.*, p. 364.
4. W. E. Moerner, *et al.*, *Phys. Rev. Lett.* **73**, 2764 (1994).
5. J. J. Macklin, J. K. Trautman, T. D. Harris, L. E. Brus, *Science* **272**, 255 (1996).
6. H. F. Hess, E. Betzig, T. D. Harris, L. N. Pfeiffer, K. W. West, *ibid.* **264**, 1740 (1994).
7. M. Nirmal, *et al.*, *Nature* **383**, 802 (1996).
8. J. E. Field, *The Properties of Diamond* (Academic Press, London, 1979).
9. J. I. Pankove and C. Qui, *Synthetic Diamond: Engineering CVD Science and Technology*, K. E. Spear and J. P. Dismukes, Eds. (Wiley, New York, 1994), pp. 401–418.
10. G. Davies and M. F. Hamer, *Proc. R. Soc. London Ser. A* **384**, 285 (1976).
11. R. T. Harley, M. J. Henderson, R. M. Macfarlane, *J. Phys. C: Solid State Phys.* **17**, L233 (1984).
12. N. R. S. Reddy, N. B. Manson, E. R. Krausz, *J. Lumin.* **38**, 46 (1987).
13. J. H. N. Loubser and J. A. van Wyk, *Rep. Prog. Phys.* **41**, 1201 (1978).
14. A. A. Kaplyanskii, *Optica Spectrosk.* **16**, 602 (1964).
15. G. Davies, *Properties and Growth of Diamond*, EMIS Data Review Series No. 9 (INSPEC, The Institution of Electrical Engineers, London, 1994).
16. A. T. Collins, M. F. Thomaz, M. I. B. Jorge, *J. Phys. C: Solid State Phys.* **16**, 2177 (1983).
17. The 514-nm line of an Ar^+ ion laser was used for fluorescence excitation. An immersion oil objective (numerical aperture-1.3; magnification, ×100) collimated the excitation light and collected the sample fluorescence. A single photon-counting silicon avalanche photodiode was used as a detector. Stray light suppression was achieved with the use of a holographic notch and a red pass filter.
18. The saturated fluorescence intensity for a single center (detection efficiency 2%) is 1.7×10^7 counts per second at an excitation intensity of 2.4 MW/cm^2.
19. J. Bernard, L. Fleury, H. Talon, M. Orrit, *J. Chem. Phys.* **98**, 850 (1993).
20. D. A. Redman, S. Brown, R. H. Sands, S. C. Rand, *Phys. Rev. Lett.* **67**, 3420 (1991).
21. D. Redman, S. Brown, S. C. Rand, *J. Opt. Soc. Am. B* **9**, 768 (1992).
22. S. P. McGlynn, T. Azumi, M. Kinoshita, *Molecular Spectroscopy of the Triplet State* (Prentice-Hall, Englewood Cliffs, NJ, 1970).
23. E. van Oort, thesis, University of Amsterdam (1990).
24. ———, P. Stroomer, M. Glasbeek, *Phys. Rev. B* **42**, 8605 (1990).
25. J. Köhler *et al.*, *Nature* **363**, 242 (1993).
26. J. Wrachtrup, C. von Borczyskowski, J. Bernard, M. Orrit, R. Brown, *ibid.*, p. 244.
27. J. Köhler, A. C. J. Brouwer, E. J. J. Groenen, J. Schmidt, *Science* **268**, 1457 (1995).
28. D. Rugar *et al.*, *ibid.* **264**, 1560 (1994).

29. We acknowledge stimulating discussions with R. Wannemacher, who pointed out the suitability of the N-V centers for single center detection. R. Pintaske supported us with the loan of a charge-coupled device camera. A. Boden and D. Bräunig from the Hahn Meitner Institute Berlin carried out the electron irradiation of the diamond samples. Support by the Deutsche Forschungsgemeinschaft through the Innovationskolleg "Methoden und Materialien für den Nanometerbereich" is gratefully acknowledged.

18 February 1997; accepted 14 April 1997

Creep Response of the Hayward Fault to Stress Changes Caused by the Loma Prieta Earthquake

James J. Lienkaemper,* Jon S. Galehouse, Robert W. Simpson

In 1996, an 18-millimeter creep event, the largest ever observed on the Hayward fault, occurred between surveys 63 days apart. This event marked the end of a period of severely reduced creep on the southern part of the fault that began after the 1989 Loma Prieta, California, earthquake. The reduction in creep was consistent with elastic models for earthquake-induced static stress changes on the Hayward fault. These data suggest that creep observations can indicate regional stress changes of about 1 bar or less.

Earthquake models generally assume that stress across plate tectonic boundaries increases steadily with time. However, large earthquakes can perturb the stress field acting on neighboring faults (*1*). We present evidence that the Loma Prieta earthquake affected the dynamics of creep on the nearby Hayward fault.

The probability of a magnitude (M) 7 or larger earthquake in the next 30 years on the Hayward fault is 45% (*2*), and it is thought to be the most hazardous fault zone in the San Francisco Bay region. The Hayward, a major branch of the San Andreas fault system, exhibits creep along at least 68 km of its <100 km length (Fig. 1). Creep rates over the past several decades vary along the fault from ~9 mm/year near the south end to ~3 mm/year in northern Oakland (*3*). The average rate for most of the fault is 4.8 mm/year (*3*). For decades before the 17 October 1989 Loma Prieta earthquake, creep rates at several monitoring sites, averaged over a few years, had gener-

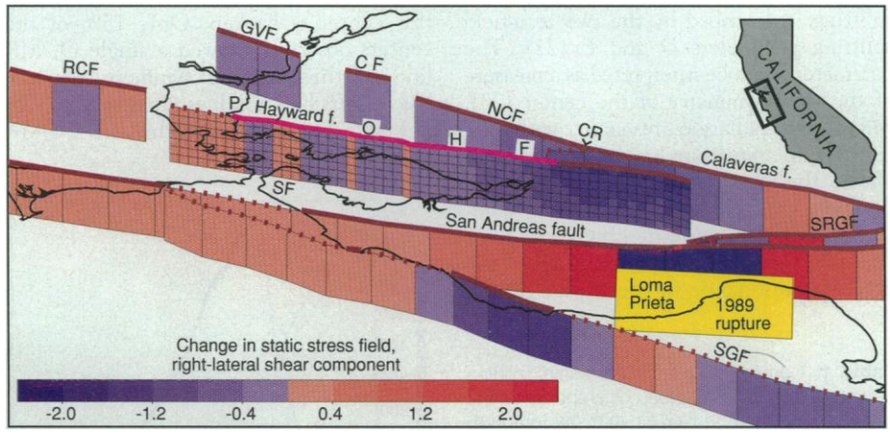

Fig. 1. Calculated static stress changes produced by Loma Prieta earthquake. Oblique view eastward of the San Francisco (SF) Bay region, California, shows the San Andreas fault system. Colored patches, mostly 10 km long by 13 km deep, show calculated changes in horizontal shear stress for each fault (*4, 5*). A red gradient indicates greater loading on a fault; blue indicates some relaxation of plate-tectonic driving stress. California map shows orientation of area in view, with the coastline in black for reference and active faults in brown. Faults are vertical, except the 1989 Loma Prieta earthquake rupture (*12*), shown in yellow, dips 70° SW. The 70-km-long, creeping Hayward fault trace is magenta; stress is computed at a grid size of 2 km. Locations: P, Point Pinole; O, Oakland; H, Hayward; F, Fremont; and CR, Calaveras Reservoir. Other faults: GVF, Green Valley; CF, Concord; NCF, Northern Calaveras; SRGF, Sargent; RCF, Rodgers Creek; and SGF, San Gregorio.